Measurement 46 (2013) 2638–2646

Contents lists available at SciVerse ScienceDirect

Measurement

journal homepage: www.elsevier.com/locate/measurement

Improved measurement accuracy in optical scatterometry using fitting error interpolation based library search

Xiuguo Chen [a], Shiyuan Liu [a,b,*], Chuanwei Zhang [b], Jinlong Zhu [a]

[a] Wuhan National Laboratory for Optoelectronics, Huazhong University of Science and Technology, Wuhan, Hubei 430074, China
[b] State Key Laboratory of Digital Manufacturing Equipment and Technology, Huazhong University of Science and Technology, Wuhan, Hubei 430074, China

ARTICLE INFO

Article history:
Received 15 January 2013
Received in revised form 23 April 2013
Accepted 29 April 2013
Available online 18 May 2013

Keywords:
Optical scatterometry
Inverse problem
Library search
Fitting error interpolation

ABSTRACT

Library search is one of the most commonly used methods for solving the inverse problem in current optical scatterometry. One issue in the conventional library search method is that its final measurement accuracy is fundamentally limited by the grid interval of each parameter in the signature library. In this paper, we propose a fitting error interpolation based library search (FEI-LS) method to improve the measurement accuracy. By comparing the interpolated fitting errors estimated in a FEI-based fine search step, the structural parameters associated with the minimum interpolated fitting error can be treated as the final measurement result. Experiments performed on a photoresist grating have demonstrated that the FEI-LS method can achieve a higher measurement accuracy for a pre-generated library without remarkable influence on the search speed. It is expected that the FEI-LS method will provide a useful and practical means for solving the inverse problem in the state-of-the-art optical scatterometry.

1. Introduction

Process control in microelectronic manufacturing requires real-time monitoring techniques. Among the different techniques, optical scatterometry, sometimes also referred to as optical critical dimension (OCD) metrology, has achieved great success in the monitoring of CD and overlay recently [1–6]. There are two main procedures in optical scatterometry. The first one involves the calculation of the optical signature from a diffractive structure using reliable forward modeling techniques, such as the rigorous coupled-wave analysis (RCWA) [7–9], the finite element method (FEM) [10,11], the boundary element method (BEM) [12], or the finite-difference time-domain (FDTD) method [13]. Here, the general term signature contains the scattered light information from the diffractive structure, which can be in the form of reflectance, ellipsometric angles, Stokes vector elements, or Mueller matrix elements. The second procedure involves the reconstruction of the structural profile from the measured signature, which is a typical inverse problem with the objective to find a profile whose calculated signature can best match the measured one.

To solve the inverse problem in optical scatterometry, several methods have been reported in recent years. Drége et al. presented a linearized method to obtain surface profile information by the linearized inversion of scatterometric data [14]. The linearized method has its inherent limitation due to the highly nonlinear relationship between the optical signature and the profile parameters. Some nonlinear regression methods, such as the Levenberg–Marquardt (LM) algorithm and its improved technique by combining with the artificial neural network (ANN) [15], have also been proposed. The nonlinear regression methods are usually time-consuming, as the structural profile is achieved through an iterative procedure that repeatedly requires computation of the forward opti-

* Corresponding author. Address: Head of Nanoscale and Optical Metrology Group, School of Mechanical Science and Engineering, Huazhong University of Science and Technology, 1037 Luoyu Road, Wuhan, Hubei 430074, China. Tel.: +86 27 8755 9543; fax: +86 27 8755 8045.
E-mail address: shyliu@mail.hust.edu.cn (S. Liu).

0263-2241/$ - see front matter © 2013 Elsevier Ltd. All rights reserved.
http://dx.doi.org/10.1016/j.measurement.2013.04.080

cal modeling. This is even worse and unacceptable when dealing with two-dimensional structures or more complex structures. A feasible way to meet the *in situ* requirement, known as library search, is to generate a signature library prior to the measurement, and then to search in the library to find a best match with the measured signature [16,17]. Although the off-line generation of the signature library is time consuming, the search itself during the on-line measurement can be done quickly with a global solution guaranteed [18]. Therefore, the library search method has been demonstrated to be an effective approach to solve the inverse problem in optical scatterometry and has been commonly used in industry [19,20].

The success of library search relies heavily on two essential aspects: the signature library and the search algorithm. In the past decades, several library search algorithms, such as the linear search, *k*-dimensional tree search, and locality-sensitive hashing, have been reported with an emphasis on the speed and accuracy of the matching result [21–23]. Besides the library search algorithm itself, the scale of the signature library is closely related to the final measurement accuracy and the speed of library search. The scale of a signature library is determined by the ranges of structural parameters and the associated grid interval (or step size) of each parameter. The ranges of structural parameters, typically depending on the process tolerances, are usually specified at ±10% of their nominal dimensions as a rule of thumb [16]. One issue in the conventional library search method is that its measurement accuracy is fundamentally limited by the grid interval. In general, the measurement accuracy of library search can be improved by decreasing the grid interval. However, it will take much more time and memory space to generate and store the signatures, and a too large size of the signature library will also greatly influence the speed of library search. Some efforts have been made to deal with this issue. Ku et al. proposed a feature region algorithm based on sensitivity analysis to reduce the size of the signature library [24]. Littau et al. investigated several techniques to determine an optimal signature scan path that can also result in a smaller signature library [25].

In this paper, we propose a fitting error interpolation based library search (FEI-LS) method to improve the measurement accuracy by interpolating on the fitting errors between the measured signature and the calculated signatures pre-stored in the library. In the FEI-LS method, a FEI-based fine search step is introduced after the coarse search in the conventional library search method. Although the signatures that are not pre-stored in the library are still unknown, their corresponding fitting errors with the measured signature can be estimated in the FEI-based fine search step. By comparing the interpolated fitting errors, the structural parameters associated with the minimum interpolated fitting error can be treated as the final measurement result. Thus, the measurement accuracy can be improved for a pre-generated library. In addition, the FEI-LS method does not care about the specific form of the signature, and the multi-dimensional interpolation on the fitting errors is only performed once in one measurement. Therefore, the FEI-LS method is also expected to have no remarkable influence on the final search speed, as the time-consuming forward modeling is completely avoided during the interpolation and library search process. We will provide sufficient details to describe the FEI-LS method, and then will report simulation and experimental results to assess its performance by comparing with other methods.

The remainder of this paper is organized as follows. Section 2 introduces the inverse problem in optical scatterometry, and then describes the FEI-LS method for solving the inverse problem. Section 3 provides some simulation and experimental results to demonstrate the higher accuracy and fast search ability of the proposed method over the conventional library search method. Finally, we draw some conclusions in Section 4.

2. Method

2.1. The inverse problem in optical scatterometry

Without loss of generality, we denote the structural parameters as an n-dimensional vector $\mathbf{x} = [x_1, x_2, \ldots, x_n]^{\mathrm{T}}$, where T represents the transposition and $x_1, x_2, \ldots, x_n$ can be the linewidth, sidewall angle, thickness, etc. The calculated signature associated with the structural parameters $\mathbf{x}$ obtained under a varying set of conditions (e.g., wavelength, incidence angle, azimuthal angle, polarization) is denoted by $\mathbf{f}(\mathbf{x})$. The corresponding measured signature is $\mathbf{y}(\mathbf{x}_0)$, where $\mathbf{x}_0$ represents the true values of the structural parameters under measurement. In practice, many kinds of metrics can be used to quantify the fitting errors between the calculated and measured signatures [26], of which the most commonly used metric, the root mean square error (RMSE), is adopted in this paper. The RMSE is defined by:

$$\chi(\mathbf{x}, \mathbf{x}_0) = \|\mathbf{f}(\mathbf{x}) - \mathbf{y}(\mathbf{x}_0)\| = \sqrt{\sum_{k=1}^{K} \omega_k [f_k(\mathbf{x}) - y_k(\mathbf{x}_0)]^2}, \qquad (1)$$

where k is the signature index, typically a wavelength or an incidence angle index in optical scatterometry. K represents the total number of signature indices, and ω_k is the weighting factor. The symbol $\chi(\mathbf{x}, \mathbf{x}_0)$ is sometimes shortened to $\chi(\mathbf{x})$ for convenience in the remainder of this paper. The inverse problem in optical scatterometry can be formulated as

$$\hat{\mathbf{x}} = \arg\min_{\mathbf{x}\in\Omega} \chi(\mathbf{x}, \mathbf{x}_0) = \arg\min_{\mathbf{x}\in\Omega} \|\mathbf{f}(\mathbf{x}) - \mathbf{y}(\mathbf{x}_0)\|, \qquad (2)$$

where $\hat{\mathbf{x}}$ is the vector containing the measured structural parameters, and Ω is the parameter domain.

2.2. The fitting error interpolation based library search

Prior to the measurement, an n-dimensional regular Cartesian grid for the structural parameters $\mathbf{x}$ ($\mathbf{x} \in \Omega$) is defined by $\mathrm{X} = \{(x_{1r}, x_{2s}, \ldots, x_{nt}): 1 \leqslant r \leqslant \tilde{r}, 1 \leqslant s \leqslant \tilde{s}, \ldots, 1 \leqslant t \leqslant \tilde{t}\}$ ($\mathrm{X} \subseteq \Omega$). The grid interval of the p-th dimension is represented by δ_p ($p = 1, 2, \ldots, n$). The calculated signature $\mathbf{f}(\mathbf{x}_i)$ associated with each discrete grid point $\mathbf{x}_i$ ($i = 1, 2, \ldots, N$; $N = \tilde{r} \times \tilde{s} \times \cdots \times \tilde{t}$) is stored in the library. Then we perform the FEI-LS to extract the structural parameters from a measured signature $\mathbf{y}(\mathbf{x}_0)$ by solving the inverse

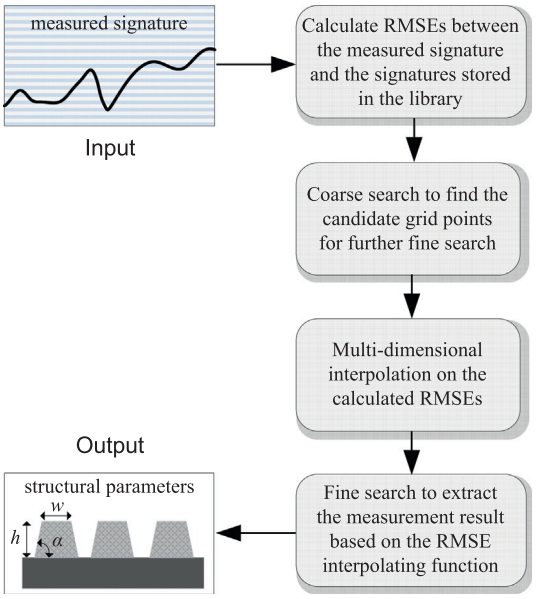

Fig. 1. Flowchart of the fitting error interpolation based library search.

problem as shown in Eq. (2). The procedure of the FEI-LS is depicted in Fig. 1 and described in detail as follows.

Step 1: The RMSEs $\chi(x_i, x_0)$ between the measured signature $\mathbf{y}(\mathbf{x}_0)$ and the calculated signatures $\mathbf{f}(\mathbf{x}_i)$ ($i = 1, 2, \ldots, N$) pre-stored in the library are calculated according to Eq. (1).

Step 2: Some search algorithm is used to scan the discrete grid points in the signature library to construct a candidate set Y ($Y \subseteq X$), of which each element (also called the candidate grid point) will be used for the subsequent fine search to find the final measurement result. This step is called coarse search in the FEI-LS method as it is quite similar to that in the conventional library search method. The main difference is that a set of several candidate grid points rather than only one candidate grid point is obtained. If the candidate set Y contains all the grid points that could be potentially close to the global minimum of $\chi(\mathbf{x}, \mathbf{x}_0)$ ($\mathbf{x} \in \Omega$), it is evident that the true values of the structural parameter $\mathbf{x}_0$ will satisfy

$$\mathbf{x}_0 \in \bigcup_{j=1}^{M} \Gamma_\gamma(\mathbf{x}_j), \tag{3a}$$

$$\Gamma_\gamma(\mathbf{x}_j) = \{\mathbf{x} \in \Omega \,\big|\, \|\mathbf{A}^{-1}(\mathbf{x} - \mathbf{x}_j)\|_\infty < \gamma\}, \quad \mathbf{x}_j \in Y, \tag{3b}$$

where $\|\cdot\|_\infty$ denotes the infinite norm. $\mathbf{A}$ is the diagonal matrix of the grid intervals, i.e., $\mathbf{A} = \mathrm{diag}(\delta_1, \delta_2, \ldots, \delta_n)$. $\Gamma_r(x_j)$ is the fine search region associated with the candidate grid point $\mathbf{x}_j$ ($\mathbf{x}_j \in Y$). M ($M < N$) represents the total number of candidate grid points contained in Y. γ is called the scaling factor of the fine search region and $0 < \gamma \leqslant 1$. A smaller scaling factor can decrease the size of the fine search region; however, a too small scaling factor may exclude the true values $\mathbf{x}_0$ from the fine search region.

Step 3: Multi-interpolation is performed upon the RMSEs associated with the grid points in the library to construct an n-dimensional RMSE interpolating function $g(\mathbf{x})$ that satisfies

$$g(\mathbf{x}_i) = \chi(\mathbf{x}_i, \mathbf{x}_0), \quad i = 1, 2, \cdots, N. \tag{4}$$

Many multi-interpolation methods such as multi-linear interpolation and multi-spline interpolation can be used in this step with different interpolation accuracy and complexity [27]. The FEI-LS method using multi-linear or multi-spline interpolation is also referred to as the linear FEI-LS or spline FEI-LS method. In addition, if $\mathbf{x}_0$ is outside the parameter domain Ω, i.e., $\mathbf{x}_0 \notin \Omega$, multi-extrapolation can sometimes be implemented to expand the pre-generated library.

Step 4: Based on the RMSE interpolating function $g(\mathbf{x})$, the inverse problem as formulated in Eq. (2) will be transformed into a constrained optimization problem

$$\hat{\mathbf{x}} = \arg\min\, g(\mathbf{x}), \quad \mathbf{x} \in \bigcup_{j=1}^{M} \Gamma_\gamma(\mathbf{x}_j). \tag{5}$$

Finally, some optimization techniques, such as the active-set, the interior-point, or the sequential quadratic programming method [28], can be implemented to find the minimum of the interpolating function $g(\mathbf{x})$. The structural parameters associated with the minimum interpolated RMSE will be treated as the final measurement result. In the iterative process, each candidate grid point in Y can be selected as the initial values of the corresponding optimization algorithm. This step is called fine search in the FEI-LS method.

It is worthwhile to point out that in the conventional library search method, the candidate set Y usually contains only one grid point with the smallest RMSE in the library, and this grid point results in a final solution as no fine search is further performed. However, it is not sufficient to just select this grid point for fine search in the FEI-LS method, because the limited grid interval might yield a local solution. As illustrated in Fig. 2 for a one-dimensional RMSE function $\chi(x)$, grid point B has the smallest RMSE in the signature library; however, further fine search around point B will lead to a local minimum point C of the RMSE function. In fact, the global minimum of $\chi(x)$ is located at point F, which is near point E. To ensure that the candidate set Y does not miss the true global minimum

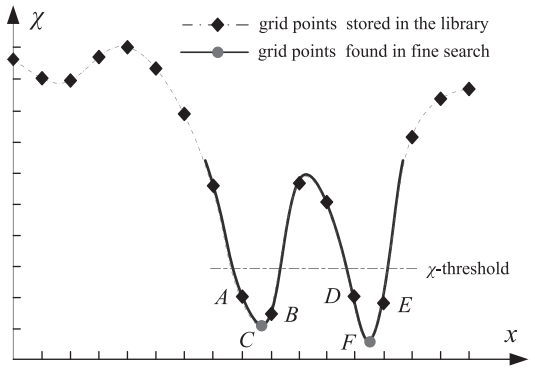

Fig. 2. An illustration of constructing the candidate set.

grid point, one approach is to set a χ-threshold in the preliminary coarse search stage. The grid points that have greater RMSEs than the setting χ-threshold are filtered out, while other grid points will be added in the candidate set. As shown in Fig. 2, the grid points *A*, *B*, *D*, and *E* will be selected for subsequent fine search by applying the χ-threshold criterion, i.e., Y = {*A*, *B*, *D*, *E*}. Alternatively, one can also directly choose the *M* grid points that correspond to the *M* smallest RMSEs in the library as the candidate grid points. The *M* smallest RMSEs can be quickly found out in the coarse search stage by using some quick sort algorithm. The candidate grid points are then provided to the fine search stage for more accurate result.

3. Results

3.1. The experimental setup

The experimental setup used in this paper is a dual-rotating-compensator ellipsometer (RC2 ellipsometer, J.A. Woollam Co.) with in-house forward modeling software based on RCWA [7–9]. As shown in Fig. 3, the system configuration of the RC2 ellipsometer in order of light propagation is $PC_{r1}(\omega_1)SC_{r2}(\omega_2)A$, where P stands for the polarizer, C_{r1} for the 1st rotating compensator, C_{r2} for the 2nd rotating compensator, S for the sample, and A for the analyzer. The 1st and 2nd compensators rotate continuously at $\omega_1 = 5\omega$ and $\omega_2 = 3\omega$, where ω is the fundamental mechanical frequency. With the light source used in this configuration, the wavelengths available are in the 193–1690 nm range including the spectral range 300–750 nm used in the paper. Data collection is performed in the specular mode, and the incidence and azimuthal angles, varied from 45° to 90° and from 0° to 360° respectively, can be chosen for maximum sensitivity. With the focusing lens, the beam diameter in the RC2 ellipsometer can be changed from normally about 3 mm to less than 200 μm. By analyzing the optical intensity signal from the spectrometer, we can obtain the reflectance, ellipsometric parameters (or Stokes vector elements), and full Mueller matrix elements of the measured sample.

As shown in Fig. 4, the sample used in the following simulations and experiments contains 35 dies. Each die consists of a photoresist grating layer (characterized by top critical dimension *TCD*, sidewall angle *SWA*, height Hgt_1, and period *pitch*) on a bottom anti-reflective coating (BARC) layer (characterized by height Hgt_2) deposited on the silicon substrate. The coordinate and sequence number of each die are shown on the left side of Fig. 4, while the profile of the grating sample is shown on the right side of Fig. 4. Nominal dimensions of the grating sample are: *TCD* = 200 nm, *SWA* = 90°, Hgt_1 = 311 nm, *pitch* = 400 nm and Hgt_2 = 115 nm. Optical properties of the BARC layer were measured in advance before the photoresist layer was coated on it. Optical properties of the silicon substrate were taken from Ref. [29]. In the selected spectral range 300–750 nm, the optical function of photoresist was modeled by the Tauc–Lorentz model [30]. The dielectric function of this model can be expressed in terms of a total of five parameters: the non-dispersive term ε_∞, the Tauc gap energy E_g, the amplitude A_{TL}, the broadening parameter C_{TL}, and the Lorentz resonant frequency E_0. The values of the above fitting parameters in our calculation are $\varepsilon_\infty = 1.3205$, $E_g = 3.9572$ eV, $A_{TL} = 29.6462$ eV, $C_{TL} = 1.4317$ eV, and $E_0 = 10.0527$ eV.

To demonstrate the validity of the proposed FEI-LS method, a signature library for the grating structure was constructed prior to the measurements. The ranges of the structural parameters *TCD*, *SWA* and Hgt_1 in the library are 160–210 nm, 85–90°, and 290–315 nm, respectively. The grating period and thickness of the BARC layer are fixed at their nominal values, *pitch* = 400 nm and Hgt_2 = 115 nm, to decrease the time consumed in the generation of the library. The grid intervals for the parameters *TCD*, *SWA* and Hgt_1 are 1 nm, 0.2° and 1 nm, respectively. Details of the signature library are listed in Table 1. The spectral range varies from 300 nm to 750 nm with an increment of 2 nm. The incidence angle is fixed at 65°, and the plane of incidence is perpendicular to the grating lines with the azimuth angle equal to 0°. The number of retained orders in the truncated Fourier series when applying RCWA to calculate the optical signatures is 12. The photoresist grating shown in Fig. 4 is sliced into 15 layers along the vertical direction. The calculated signatures stored in the library are in the forms of Stokes vector elements S_1, S_2, S_3, which are defined by

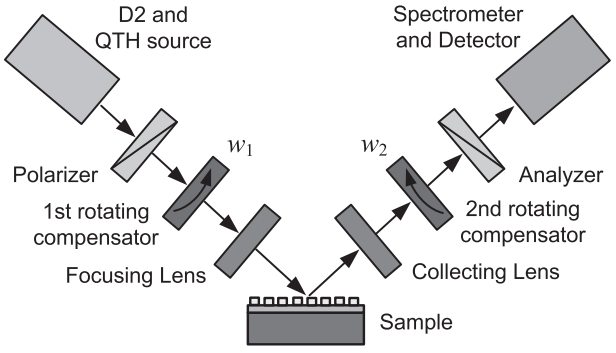

Fig. 3. Basic scheme of the dual-rotating compensator ellipsometer used in the experiments.

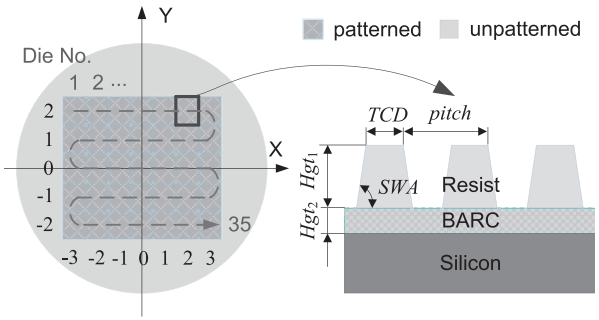

Fig. 4. Schematic diagram of the grating structure used in the simulations and experiments.

$$S_1 = \cos 2\psi, \quad S_2 = \sin 2\psi \cos \Delta, \quad S_3 = \sin 2\psi \sin \Delta, \qquad (6)$$

where ψ and Δ are the ellipsometric angles.

3.2. Simulation results

Before the experiments, we performed some simulations to investigate the possible influences on the performance of the FEI-LS method, including the scaling factor γ ($0 < \gamma \leqslant 1$) of the fine search region as described in Eq. (3b), the candidate set Y that contains the grid points for further fine search, and the interpolation method (mainly the multi-linear interpolation and multi-spline interpolation) performed on the fitting errors. The final measurement accuracy in the simulations is assessed by

$$\varepsilon_l = \left|\hat{\mathbf{x}}^{(l)} - \mathbf{x}_0^{(l)}\right|, \quad \bar{\varepsilon} = \frac{1}{L}\sum_{l=1}^{L}\varepsilon_l, \qquad (7)$$

where ε_l represents the absolute error for the lth test. $\bar{\varepsilon}$ is the mean absolute error for the total number of L tests. $\mathbf{x}_0^{(l)}$ and $\hat{\mathbf{x}}^{(l)}$ are the given and extracted structural parameters for the lth test, respectively.

We randomly generated 100 groups of structural parameters ($L = 100$) within the range of each parameter in the library as described in Table 1. The calculated signature associated with each group of structural parameters was treated as the "measured" signature. The FEI-LS method was then implemented to extract the structural parameters from the pre-generated library for the "measured" signatures. Fig. 5 depicts the comparison of the mean absolute errors of the extracted parameters *TCD*, Hgt_1 and *SWA* by the spline FEI-LS method with different scaling factors and candidate sets containing different number of grid points. From Fig. 5, it is clear that when the scaling factor and the number of candidate grid are too small, they indeed have remarkable influence on the measurement accuracy of the FEI-LS method. When the scaling factor $\gamma \geqslant 1/2$ and the number of candidate grid points $M \geqslant 10$, the measurement accuracy of the FEI-LS method tends towards stability. Considering that a too large scaling factor and a too large number of candidate grid points may decrease the search speed of the FEI-LS method, we choose $\gamma = 1/2$ and $M = 10$ in the following simulations and experiments. It should be noted that there might be minor differences in the values of γ and M in different measurement conditions and for different samples. However, we can safely derive the values of γ and M in other applications by performing similar simulations as depicted in Fig. 5. Fig. 6 depicts the comparison of the mean absolute errors of the extracted parameters *TCD*, Hgt_1 and *SWA* by the linear and spline FEI-LS methods respectively. We can observe from Fig. 6 that the measurement accuracy of the spline FEI-LS method is much higher than that of the linear FEI-LS method. This is because the relationship between the fitting errors and the structural parameters is usually nonlinear, and the linear interpolation cannot give a good prediction about the distribution of the minima of the actual fitting error function $\chi(\mathbf{x}, \mathbf{x}_0)$ ($\mathbf{x} \in \Omega$).

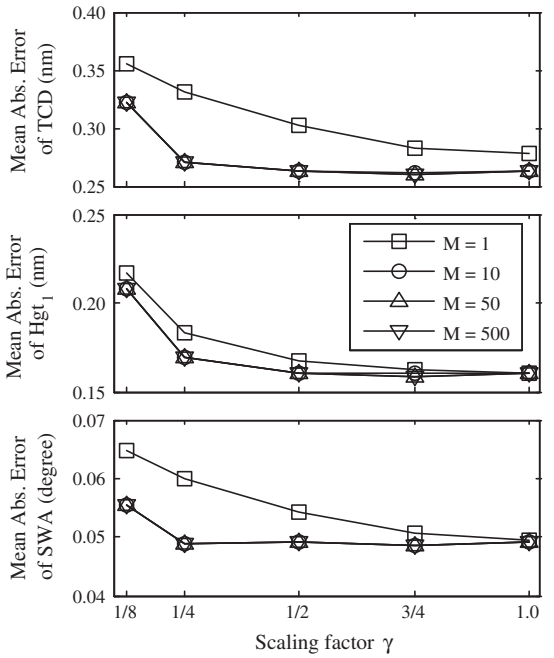

Fig. 5. Comparison of the mean absolute errors of parameters *TCD*, Hgt_1 and *SWA* extracted by the spline FEI-LS method with different scaling factors γ and different number of candidate points *M*.

In order to compare the measurement accuracy of the proposed FEI-LS method to the conventional library search method, we generated another 50 groups of structural

Table 1
Details of the signature library used in the simulations and experiments.

Parameter name	Nominal dimension	Lower bound	Upper bound	Grid interval	Number of grids	Library size (no. of signatures)
TCD	200 nm	160 nm	210 nm	1 nm	51	$51 \times 26 \times 26 = 34{,}476$
Hgt_1	311 nm	290 nm	315 nm	1 nm	26	
SWA	90°	85°	90°	0.2°	26	

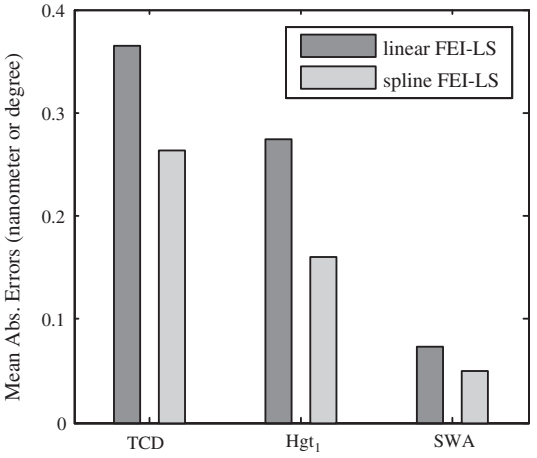

Fig. 6. Comparison of the mean absolute errors of parameters *TCD*, Hgt_1 and *SWA* extracted by the linear and spline FEI-LS methods with the scaling factor fixed at $\gamma = 1/2$ and the number of candidate points being $M = 10$.

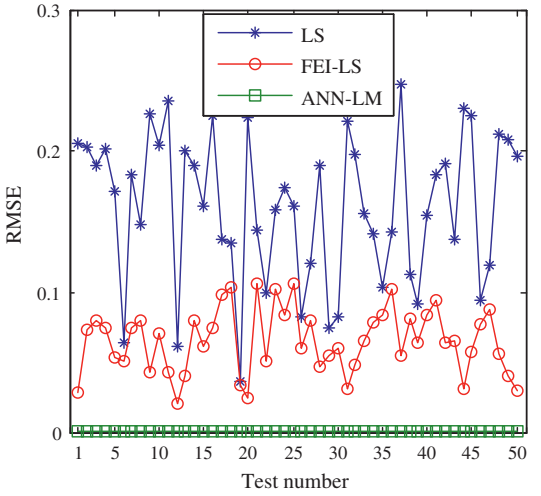

Fig. 8. RMSEs between the "measured" and calculated signatures obtained by the conventional library search (LS) and FEI-LS methods for the 50 tests.

parameters ($L = 50$) randomly within the range of each parameter in the library as described in Table 1. The calculated signature associated with each group of structural parameters was also treated as the "measured" signature. The spline FEI-LS method was applied to make this comparison with the scaling factor $\gamma = 1/2$ and the number of candidate grid points $M = 10$. Fig. 7 depicts the absolute errors of the extracted parameters *TCD*, *SWA* and Hgt_1 for the 50 tests, and the mean absolute error for each parameter is

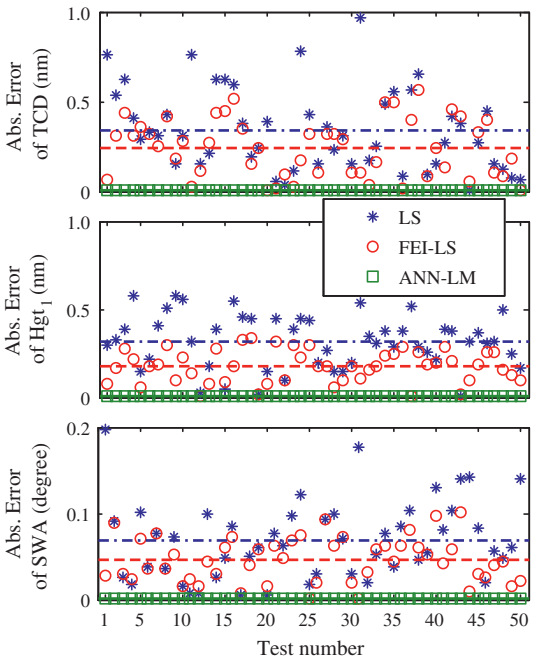

Fig. 7. Absolute errors of the extracted parameters *TCD*, Hgt_1 and *SWA* for the 50 tests, with the dash-dotted and dashed lines denoting the mean absolute errors obtained by the conventional library search (LS) and FEI-LS methods respectively.

inserted in the corresponding sub-figure. It is observed from Fig. 7 that a higher measurement accuracy is achieved for the pre-generated signature library by applying the FEI-LS method. Fig. 8 shows the RMSEs between the "measured" signature and the calculated signatures that correspond to the finally extracted parameters by the conventional library search and FEI-LS methods. It is obvious that the RMSEs calculated by the FEI-LS method are less than those by the conventional library search method due to the interpolation-based fine search that is performed to further reduce the RMSE. Consequently, a better match between the "measured" and calculated signatures for a pre-generated library can be achieved by using the FEI-LS method.

3.3. Experimental results

The grating sample shown in Fig. 4 was measured die by die by using the RC2 ellipsometer. The FEI-LS, conventional library search, and LM algorithm were then performed to extract the structural parameters for the measured signatures. In the FEI-LS method, the three-dimensional spline interpolation upon the RMSEs was performed with the scaling factor $\gamma = 1/2$ and the number of candidate grid points $M = 10$. Since the true values $\mathbf{x}_0$ of the structural parameters associated with the measured signatures are unknown, we use the measurement result of the LM algorithm as a reference to compare the measurement accuracy of the FEI-LS and conventional library search methods. It is well known that the LM algorithm can achieve very accurate results if there is convergence. However, the measurement results of the LM algorithm are very sensitive to the initial starting point used in the iteration. An improper starting point for the LM algorithm may lead to a local solution. In our previous work, an ANN and LM combined algorithm was proposed for solving the inverse problem in reflectometry [15]. In the ANN-LM combined algorithm, an initial estimate of the structural

parameters is quickly generated from the measured signature by the ANN, and then the accurate result is further obtained by the LM algorithm. It was demonstrated that the combined extraction algorithm can achieve improved performance over the ANN or LM algorithm alone and can lead to highly accurate measurement results.

In our experiments, we first used the pre-generated signature library as depicted in Table 1 as a training set to train a back-propagation neural network, and then input the measured signatures into the trained network. The mapping results of the neural network were selected as the initial values of the LM algorithm for further parameter extraction. In order to examine the validity of taking the measurement result of the ANN-LM algorithm as the reference, we applied the ANN-LM algorithm to extract the structural parameters from the "measured" signatures associated with the generated 50 groups of structural parameters in Figs. 7 and 8. The absolute errors of the extracted parameters *TCD*, *SWA* and Hgt_1 by the ANN-LM algorithm are also presented in Fig. 7. The mean absolute errors for *TCD*, Hgt_1 and *SWA* are 1.25×10^{-7} (nm), 4.11×10^{-8} (nm) and 2.97×10^{-8} (degree) respectively, which are errors in numerical calculation. The RMSEs between the "measured" signatures and the calculated signatures that correspond to the finally extracted parameters by the ANN-LM algorithm are shown in Fig. 8. The corresponding mean RMSE is 2.53×10^{-8}. According to Figs. 7 and 8, we observe that the ANN-LM algorithm indeed achieves highly accurate results. In the above simulations, the "measured" signatures are ideal and there are no errors in them, therefore the ANN-LM algorithm could converge to the true solution. However, the actually measured signatures inevitably have errors. It is therefore also necessary to compare the measurement results of the ANN-LM algorithm with other measurement approaches, such as atomic force microscope (AFM) and scanning electron microscope (SEM). In the experiments, we compared the measurement results of the ANN-LM algorithm with those measured by SEM, and good agreements have been found. Finally, we can conclude that it is suitable to take the measurement result of the ANN-LM algorithm as the reference to evaluate the final measurement accuracy of the library search methods.

Fig. 9 depicts the absolute errors of the extracted parameters *TCD*, Hgt_1 and *SWA* for each die of the grating sample shown in Fig. 4. The mean absolute error associated with each structural parameter is inserted in the corresponding sub-figure. It is noted from Fig. 9 that the final measurement accuracy is indeed dramatically improved by using the proposed FEI-LS method. A comparison between Figs. 7 and 9 also reveals that the accuracy improvement using the FEI-LS method is much more pronounced in Fig. 9. It may be because the measurement accuracy of the FEI-LS method is different for samples with different structural parameters due to the interpolation errors just as shown in Fig. 7. In addition, the structural parameters corresponding to samples in Fig. 7 vary within a comparatively larger range than the structural parameters corresponding to different dies in Fig. 9 do. Fig. 7 reveals the overall measurement accuracy of the FEI-LS method, while Fig. 9 presents the measurement accuracy in a relatively small parameter range. Anyway, the results shown in Figs. 7 and 9 demonstrate that a much higher measurement accuracy is indeed achieved by using the FEI-LS method. As an example, Table 2 shows the extracted parameters for the No. 9 die with coordinate (−2, 1) as shown in Fig. 4. Fig. 10 depicts the measured Stokes vector elements and the fitted Stokes vector elements calculated from the extracted parameters shown in Table 2 by the conventional library search, FEI-LS, and ANN-LM algorithm respectively. Although it is not so obvious in Fig. 10a, it indeed can be observed in Fig. 10b that the ANN-LM combined algorithm achieves the lowest fitting error, the FEI-LS method almost has the same fitting performance to the ANN-LM combined algorithm, and both of them outperform the conventional library search method. This experimental observation confirms again that a better match between the measured and calculated signatures for a pre-generated library can be achieved by using the FEI-LS method.

The time cost of different methods including the conventional library search, FEI-LS, and ANN-LM algorithm in the parameter extraction was also evaluated in the experiments. Fig. 11 depicts the time cost for the 35 dies of the

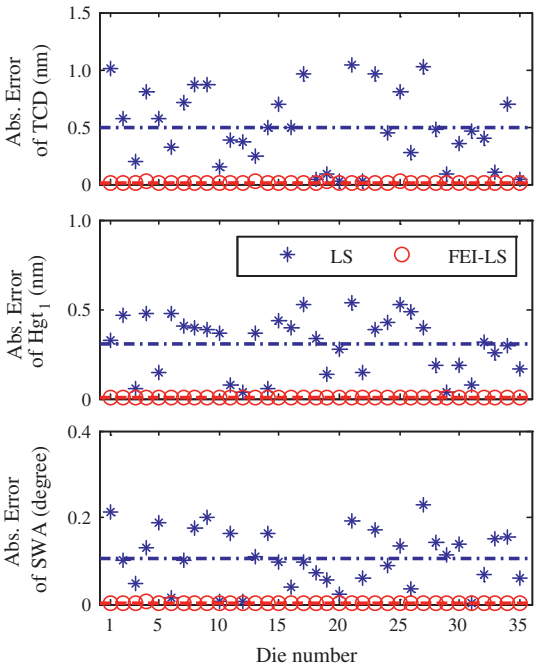

Fig. 9. Absolute errors of the extracted parameters *TCD*, Hgt_1 and *SWA* for the 35 dies of the grating sample shown in Fig. 4, with the dash-dotted and dashed lines denoting the mean absolute errors obtained by the conventional library search (LS) and FEI-LS methods respectively.

Table 2
Comparison of the parameters extracted by the conventional library search (LS), FEI-LS, and ANN-LM combined algorithm.

Algorithm	*TCD* (nm)	Hgt_1 (nm)	*SWA* (degree)	RMSE
LS	166	300	88.8	1.8270086
FEI-LS	166.8814	299.6207	89.0020	1.8171524
ANN-LM	166.8743	299.6193	89.0002	1.8171520

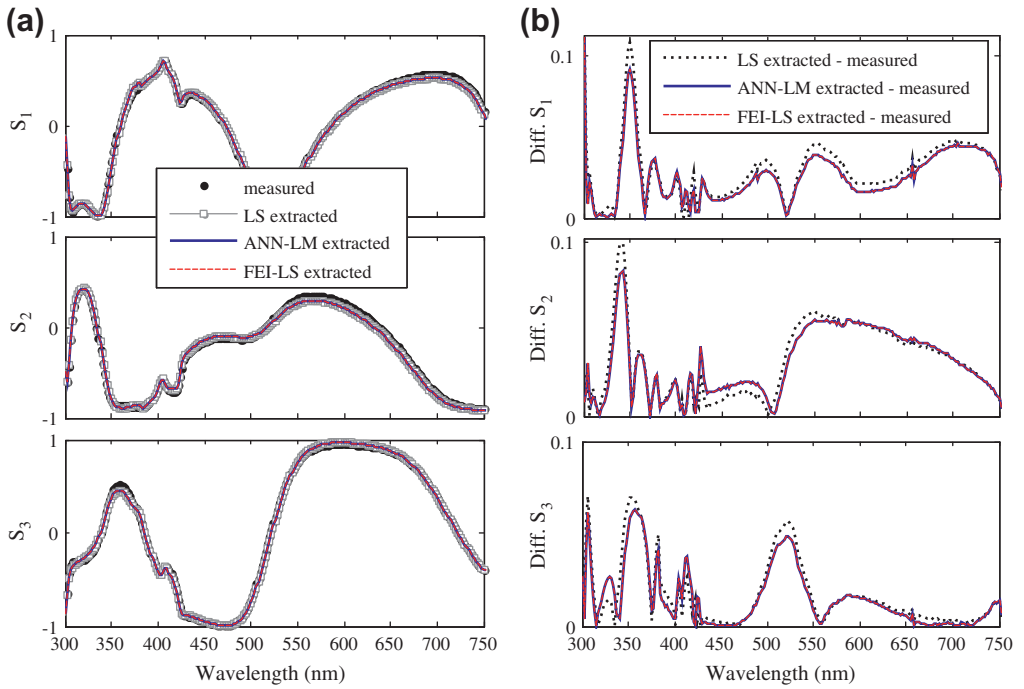

Fig. 10. (a) The measured Stokes vector elements for No. 9 die of the grating sample shown in Fig. 4 and the fitted Stokes vector elements calculated from the extracted parameters presented in Table 2 by the conventional library search (LS), FEI-LS, and ANN-LM combined algorithm; and (b) the fitting errors between the calculated and measured Stokes vector elements.

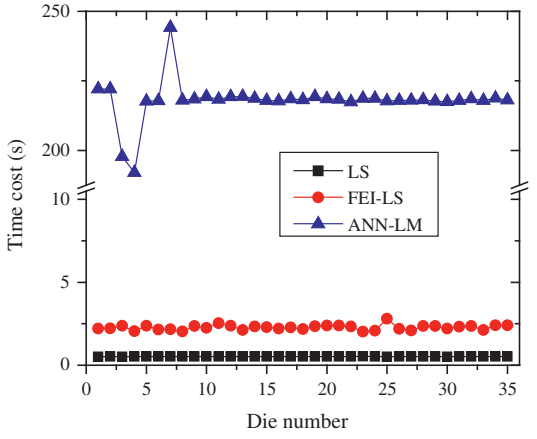

Fig. 11. Time cost of the conventional library search (LS), FEI-LS, and ANN-LM combined algorithm in the parameter extraction.

grating sample on a 3.64 GHz Xelon workstation (HP Z800). The mean time cost for the 35 dies is 0.522s by the conventional library search method, 2.278s by the proposed FEI-LS method, and 217.802s by the ANN-LM combined algorithm, respectively. As expected, the FEI-LS method is much faster than the ANN-LM algorithm, but is slightly slower than the conventional library search method. This is because that besides the library search itself, some extra time has to be spent for the multiple-interpolation and related fine search operations in the FEI-LS method. In our experiments, this extra time has been demonstrated to be on the same order of the library search itself, leading to no remarkable influence on the final search speed by the FEI-LS method. It is also worthwhile to point out that in our experiments, the multi-interpolation upon the RMSEs and the solution of the constrained optimization problem as formulated in Eq. (5) were conducted in MATLAB® by using the "interpn" and "fmincon" functions respectively. The "interpn" function was repeatedly called to calculate the RMSEs associated with the adjusted structural parameters during each iterative process of the "fmincon" function. Assuming that the complexity of the "interpn" function is $O(m)$, the complexity of the FEI-LS method will be $O(km)$, where k represents the total number of iterations of the "fmincon" function. Further improvement for the FEI-LS method may be achieved by constructing the RMSE interpolating function prior to the iteration. Then, the RMSEs associated with the adjusted structural parameters in each iteration can be directly obtained from the pre-constructed RMSE interpolating function. In this way, the multi-interpolation will be only performed one time in the process of solving the constrained optimization problem, and the complexity of the FEI-LS method will be reduced to $O(m)$. Consequently, we can conclude that the proposed FEI-LS method can be used for solving the inverse problem in optical scatterometry with a higher measurement accuracy and without remarkable influence on the search speed.

4. Conclusions

The library search is one of the most commonly used methods for solving the inverse problem in current optical

scatterometry. One issue in the conventional library search method is that its final measurement accuracy is fundamentally limited by the grid interval of each parameter in the signature library. In this paper, an interpolation based library search method termed fitting error interpolation based library search (FEI-LS) has been proposed in sufficient details. Simulations and experiments conducted on a photoresist grating on a BARC layer deposited on the silicon substrate have confirmed that a higher measurement accuracy can be achieved for a pre-generated library by applying the proposed FEI-LS method. It has also been observed that the measurement accuracy of the FEI-LS method is in good agreement with that of the ANN-LM combined algorithm, but the FEI-LS method is much faster than the ANN-LM algorithm. In addition, the extra time cost in the multi-interpolation and related fine search operations in the FEI-LS method has been demonstrated to be on the same order of the conventional library search method. It is therefore expected that the FEI-LS method will provide a useful means for solving the inverse problem in optical scatterometry with a higher measurement accuracy and without remarkable influence on the final search speed.

Acknowledgements

The authors wish to acknowledge the financial support from the National Natural Science Foundation of China (Grant Nos. 91023032, 51005091, and 51121002) and the National Instrument Development Specific Project of China (Grant No. 2011YQ160002).

References

[1] C.J. Raymond, M.R. Murnane, S. Sohail, H. Naqvi, J.R. McNeil, Metrology of subwavelength photoresist gratings using optical scatterometry, J. Vac. Sci. Technol. B 13 (1995) 1484–1495.
[2] B.K. Minhas, S.A. Coulombe, S. Sohail, H. Naqvi, J.R. McNeil, Ellipsometric scatterometry for metrology of sub-0.1 μm-linewith structures, Appl. Opt. 37 (1998) 5112–5115.
[3] C.H. Ko, Y.S. Ku, Overlay measurement using angular scatterometer for the capability of integrated metrology, Opt. Express 14 (2006) 6001–6010.
[4] R.M. Al-Assaad, S. Regonda, L. Tao, S.W. Pang, W.C. Hu, Characterizing nanoimprint profile shape and polymer flow behavior using visible light angular scatterometry, J. Vac. Sci. Technol. B 25 (2007) 2396–2401.
[5] M. El Kodadi, S. Soulan, M. Besacier, P. Schiavone, Real time scatterometry for profile control during resist trimming process, J. Vac. Sci. Technol. B 27 (2009) 3232–3237.
[6] J. Li, J.J. Hwu, Y. Liu, S. Rabello, Z. Liu, J. Hu, Mueller matrix measurement of asymmetric gratings, J. Micro/Nanolith. MEMS MOEMS 9 (2010) 041305.
[7] M.G. Moharam, E.B. Grann, D.A. Pommet, T.K. Gaylord, Formulation for stable and efficient implementation of the rigorous coupled wave analysis of binary gratings, J. Opt. Soc. Am. A 12 (1995) 1068–1076.
[8] L. Li, Use of Fourier series in the analysis of discontinuous periodic structures, J. Opt. Soc. Am. A 13 (1996) 1870–1876.
[9] S.Y. Liu, Y. Ma, X.G. Chen, C.W. Zhang, Estimation of the convergence order of rigorous coupled-wave analysis for binary gratings in optical critical dimension metrology, Opt. Eng. 51 (2012) 081504.
[10] H. Gross, R. Model, M. Bär, M. Wurm, B. Bodermann, A. Rathsfeld, Mathematical modelling of indirect measurements in scatterometry, Measurement 39 (2008) 782–794.
[11] J. Pomplun, F. Schmidt, Accelerated a posterior error estimation for the reduced basis method with application to 3D electromagnetic scattering problems, SIAM J. Sci. Comput. 32 (2010) 498–520.
[12] Y. Nakata, M. Kashiba, Boundary-element analysis of plane-wave diffraction from groove-type dielectric and metallic gratings, J. Opt. Soc. Am. A 7 (1990) 1494–1502.
[13] H. Ichikawa, Electromagnetic analysis of diffraction gratings by the finite-difference time-domain method, J. Opt. Soc. Am. A 15 (1998) 152–157.
[14] E. Drége, J. Reed, D. Byrne, Linearized inversion of scatterometric data to obtain surface profile information, Opt. Eng. 41 (2002) 225–236.
[15] C.W. Zhang, S.Y. Liu, T.L. Shi, Z.R. Tang, Improved model-based infrared reflectrometry for measuring deep trench structures, J. Opt. Soc. Am. A 26 (2009) 2327–2335.
[16] C.J. Raymond, Scatterometry for semiconductor metrology, in: A.C. Diebold (Ed.), Handbook of Silicon Semiconductor Metrology, Marcel Dekker, New York, 2001, pp. 477–514.
[17] X. Niu, N. Jakatdar, J. Bao, C.J. Spanos, Specular spectroscopic scatterometry, IEEE Trans. Semicond. Manuf. 14 (2001) 97–111.
[18] C.J. Raymond, M. Littau, A. Chuprin, S. Ward, Comparison of solutions to the scatterometry inverse problems, Proc. SPIE 5375 (2004) 564–575.
[19] P. Thony, D. Herisson, D. Henry, E. Severgnini, M. Vasconi, Review of CD measurement and scatterometry, AIP Conf. Proc. 683 (2003) 381–388.
[20] C. Raymond, Overview of scatterometry applications in high volume silicon manufacturing, AIP Conf. Proc. 788 (2005) 394–402.
[21] J.L. Bentley, Multidimensional binary search trees used for associative searching, Commun. ACM 18 (1975) 509–517.
[22] D.T. Lee, C.K. Wong, Worst-case analysis for region and partial region searches in multidimensional binary search trees and balanced quad trees, Acta. Inform. 9 (1977) 23–29.
[23] A. Gionis, P. Indyk, P. Motwani, Similarity search in high dimensions via hashing, Proc. VLDB (1999) 518–529.
[24] Y.S. Ku, S.C. Wang, D.M. Shyu, N. Smith, Scatterometry-based metrology with feature region signatures matching, Opt. Express 14 (2006) 8482–8491.
[25] M. Littau, D. Forman, J. Bruce, C.J. Raymond, S.G. Hummel, Diffraction signature analysis methods for improving scatterometry precision, Proc. SPIE 6152 (2006) 615236.
[26] R.R. Nidamanuri, B. Zbell, A method for selecting optimal spectral resolution and comparison metric for material mapping by spectral library search, Prog. Phys. Geog. 34 (2010) 47–58.
[27] W.H. Press, S.A. Teukolsky, W.T. Vetterling, B.P. Flannery, Numerical Recipes: The Art of Scientific Computing, third ed., Cambridge University Press, New York, 2007.
[28] J. Nocedal, S.J. Wright, Numerical Optimization, second ed., Springer, New York, 2006.
[29] C.M. Herzinger, B. Johs, W.A. McGahan, J.A. Woollam, W. Paulson, Ellipsometric determination of optical constants for silicon and thermally grown silicon dioxide via a multi-sample, multi-wavelength, multi-angle investigation, J. Appl. Phys. 83 (1998) 3323–3336.
[30] G.E. Jellison, F.A. Modine, Parameterization of the optical functions of amorphous materials in the interband region, Appl. Phys. Lett. 69 (1996) 371–373.